Research Square

Preprints are preliminary reports that have not undergone peer review.
They should not be considered conclusive, used to inform clinical practice,
or referenced by the media as validated information.

Zn^{2+} Content-Dependent Structural, Magnetic, and Electrochemical Properties of MgSrZn x Fe 2 O 4 Nanoferrites for Electromagnetic and Energy-Storage Applications

K. Kumar

kumaranphy@gmail.com

Shree Shanmugha college of Engineering and Technology (Autonomous)

N. Sengottaian

Excel Engineering College (Autonomous)

A. Sivakumar

Karpagam Academy of Higher Education

P. Arulmozhi

Gnanamani College of Technology (Autonomous)

Research Article

Keywords: Ferrite, MgSrZn□Fe2O4, high magnetization, Nano-rod, Trasatti

Posted Date: November 20th, 2026

DOI: https://doi.org/10.21203/rs.3.rs-11522810/v1

License: This work is licensed under a Creative Commons Attribution 4.0 International License.
Read Full License

Additional Declarations: No competing interests reported.

Zn^{2+} Content-Dependent Structural, Magnetic, and Electrochemical Properties of $MgSrZn_xFe_2O_4$ Nanoferrites for Electromagnetic and Energy-Storage Applications

K. Kumar[a*], N. Sengottaian[b], A. Sivakumar[c], P. Arulmozhi[d]

[a]Department of Physics, Shree Shanmugha college of Engineering and Technology (Autonomous), Sankari, Namakkal (Dt)-637304, Tamil Nadu-India.

[b]Department of Civil Engineering, Excel Engineering College (Autonomous), Komarapalayam, Namakkal (Dt)-637303, Tamil Nadu-India.

[c]Department of Mechanical Engineering, Centre for Material Science, Karpagam Academy of Higher Education,Coimbatore – 641021, Tamil Nadu-India.

[d]Department of Mechanical Engineering, Gnanamani College of Technology (Autonomous), Namakkal (Dt)-637018, Tamil Nadu-India.

Abstract

The ferrite materials $MgSrZn_xFe_2O_4$ (x = 0.00, 0.05, 0.10, 0.15 and 0.20) were synthesized and systematically studied to clarify the impact of Zn substitution on the structural, morphological, magnetic and electrochemical properties. The surface morphology of prepared samples was analysed by using FESEM and it was found that the particles were found to be primarily irregular and agglomerated in nature. The $MgSrZn_{0.15}Fe_2O_4$ composition had additional elongated rod-like properties. The EDS analysis revealed the presence of Mg, Zn, Sr, Fe and O, which are in agreement with the elemental composition of synthesized ferrite system. The magnetic studies showed a strong association of the magnetic response with the Zn level. Among the studied compositions, the composition $MgSrZn_{0.15}Fe_2O_4$ showed a high saturation magnetization of 157.53 emu g^{-1} and a coercivity of 67.60 Oe, indicating a favorable combination of high magnetization and relatively low coercive field. The electrochemical properties were further investigated by using 1M Na_2SO_4 solution. The $MgSrZn_{0.15}Fe_2O_4$ electrode shows a specific capacitance of 271 F g^{-1} at 5 mV s^{-1} by cyclic voltammetry and 372 F g^{-1} at 1.5 A g^{-1} by galvanostatic charge-discharge measurements. The Trasatti study suggested that the process was mostly inner/diffusion-controlled and the kinetic investigation based on scan-rate showed an increasing surface-controlled effect at high scan-rates. The tunable magnetic properties together with the large electrochemical charge storage capacity show the potential of $MgSrZn_xFe_2O_4$ ferrites for magnetic and electrochemical applications.

Keywords: Ferrite, $MgSrZn_xFe_2O_4$, high magnetization, Nano-rod, Trasatti.

Corresponding Author: K.Kumar**; E-Mail Id:** kumaranphy@gmail.com;

Ph.No: +91 8344185554

1. Introduction

The growing global energy crisis caused by the depletion of fossil fuel resources and the increasing environmental impacts of greenhouse gas emissions have resulted in an urgent search for sustainable and efficient energy storage and conversion solutions [1-3]. Renewable energy sources, including solar and wind power, are intermittent, thereby stressing the critical importance of sophisticated energy storage technology for grid stability and reliability [4, 5]. Supercapacitors have been seen as promising alternatives among different electronic energy storage devices due to their high-power density, fast charge-discharge performance, long cycle life and improved safety compared to conventional batteries [6-8]. However, the relatively low energy density of supercapacitors is a fundamental bottleneck limiting their wide applications [9,10]. Hence, a lot of research work is aimed at fabricating new electrode materials with enhanced electrochemical (EC) performance to establish a link between batteries and classic capacitors [11,12].

Spinel ferrites with general formula MFe_2O_4 ('M'= divalent metal cation) have drawn a growing interest in the quest for better electrode materials owing to their unique structural, electrical and magnetic properties, cheapness, eco-friendliness and chemical stability [13-15]. Magnesium ferrite ($MgFe_2O_4$) has been investigated for supercapacitor applications due to its good redox properties and enough specific capacitance [16]. It has been reported that $MgFe_2O_4$ nanoparticles prepared by combustion techniques exhibit a specific capacitance of 563 F g^{-1} at 0.1 A g^{-1}, indicating their possible application as low-cost electrode materials [17]. Furthermore, the role of the current collector in the electrochemical performance of chemically synthesized $MgFe_2O_4$ has been demonstrated. For example, nickel foam delivers the excellent EC performance with a specific capacitance of 298 F g^{-1} and 90 % capacitance retention after 3000 cycles [18]. However, the widespread application of pure $MgFe_2O_4$ is often hindered by its relatively poor electrical conductivity and limited reactive surface area [19].

To overcome these drawbacks, cation substitution has been shown to be effective to tune the physicochemical properties of spinel ferrites. Substitution of heterovalent or isovalent cations can cause lattice distortion, alter the cation distribution between tetrahedral and octahedral sites, enhance electrical conductivity, and create oxygen vacancies as additional electroactive sites to perform electrochemical reactions [20, 21]. For example, the integration

of palladium in $MgFe_2O_4$ was found to boost the structural stability and electrochemical performance, and chromium doping was explored to improve the performance of supercapacitor electrodes [22, 23]. Among various dopants, zinc (Zn^{2+}) prefers to occupy the tetrahedral sites in the spinel lattice. This alters the redistribution of cations and leads to a significant change in electrical and magnetic properties [24–26].

The Zn^{2+} doping in magnesium-strontium (Mg-Sr) nanoferrites is anticipated to playa curial role in their properties for energy storage applications. The incorporation of Zn^{2+} could results in a reduction in the magnetocrystalline anisotropy and a change in the saturation magnetization, which are closely related to the electronic structure and charge transfer behavior of the material [27,28]. The recent study on Zn^{2+}-doped Mg-Cu ferrites ($Mg_{0.5}Zn_xCu_{0.}$-xFe_2O_4) showed a strong link between the specific capacitance and Zn^{2+} concentration, and the optimum composition achieved a specific capacitance of 192.5 F g^{-1} at 1.75 A g^{-1} under 1 M KOH electrolyte [29]. This improvement was attributed to the change in surface area, pore size and cation distribution under the doping of Zn^{2+}. The selective occupation of the tetrahedral sites by Zn^{2+} ions can change the concentration of Fe^{3+} ions at the octahedral sites, affecting the redox behavior and overall electrochemical efficiency of the ferrite [30].

Although the improved electrical and magnetic characteristics for induction applications of Co^{2+} substituted Mg-Sr nanoferrites have been demonstrated in the literature [31], no detailed investigation has been implemented on the effect of Zn^{2+} concentration on the structural, electrical, supercapacitor, and magnetic properties of Mg-Sr nanoferrites. The systematic study of Zn^{2+} substitution in this system is vital in understanding the structure-property relationship and improving the material for multi-functional applications especially in energy storage. In this paper, we have studied the properties of Mg-Sr nanoferrites with different Zn^{2+}contents focusing on the correlation between the cation distribution and the resulting structural, electrical, supercapacitive and magnetic properties. The results of the present study are likely to offer considerable insight into the development of efficient and affordable spinel ferrite materials for future supercapacitor applications and other advanced technologies.

2. Materials and Methods

2.1 Materials

Metal-ion precursors for the synthesis of $MgSrZn_xFe_2O_4$ nanoparticles: ferric nitrate nonahydrate ($Fe(NO_3)_3{\cdot}9H_2O$), zinc nitrate hexahydrate ($Zn(NO_3)_2{\cdot}6H_2O$), strontium nitrate

($Sr(NO_3)_2$) and Magnesium nitrate hexahydrate ($Mg(NO_3)_2 \cdot 6H_2O$). The pH was adjusted by modifying the solution using sodium hydroxide (NaOH) as a precipitating agent. Deionized water and ethanol were used for preparation of precursors and washing, respectively. All chemicals were of analytical purity and were used as such without further purification.

2.2 Synthesis of $MgSrZn_xFe_2O_4$ nanoparticles

Precipitation method was utilized to synthesize $MgSrZn_xFe_2O_4$ nanoparticles. To obtain perfect homogeneity, sufficient amounts of magnesium nitrate hexahydrate ($Mg(NO_3)_2 \cdot 6H_2O$, 0.16mol), ferric nitrate nonahydrate ($Fe(NO_3)_3 \cdot 9H_2O$, 0.40mol), strontium nitrate ($Sr(NO_3)_2$, 0.04mol) and zinc nitrate hexahydrate ($Zn(NO_3)_2 \cdot 6H_2O$, 0.04-Xmol) were dissolved in 1hour. The precursor solution was heated to 90 °C on a hot plate and then 6 mol NaOH solution was added dropwise while stirring frequently until the pH reached 13 where precipitation started. The precipitate was collected and washed thoroughly several times with ethanol and distilled water to remove unreacted precursors and soluble impurities. The precipitate was then dried in a hot air oven at 90 °C for 6 hrs. Finally, the solid $MgSrZn_xFe_2O_4$ nanoparticles were obtained by calcination of the dry precursor at 900 °C in air for 3 h.

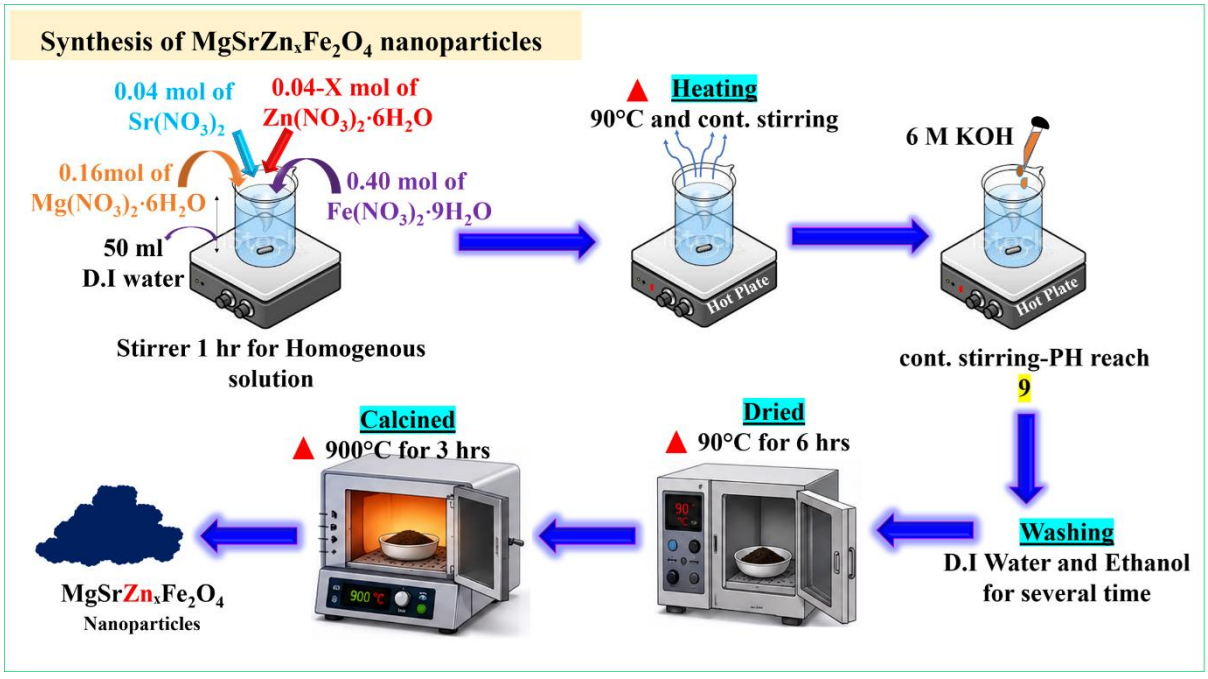

Fig.1. Schematic representation of $MgSrZn_xFe_2O_4$ synthesis procedure.

2.3 Instrumentation

Various approaches have been used to characterize the produced $MgSrZn_xFe_2O_4$ nanoparticles. PerkinElmer Diamond/NETZSCH STA 449 F3 instrument used to analysed

thermal stability (TGA/DTA; heating rate -20 °C min^{-1}). PerkinElmer Spectrum RXI spectrometer used to analyse FTIR spectra (range 4000-400 cm^{-1}) prepared materials. The phase composition and the crystallite characteristics were investigated by XRD using an X'PERT PRO-PANalytical PHILIPS diffractometer with Cu Kα radiation. The morphological properties were investigated by SEM (JSM-6610LV) and TEM (JEM-2100). Lake Shore 7404 VSM and Versa STAT MC spectrometer (impedance properties record; 1 HZ to 1 MHz) used to analyse magnetic properties of prepared materials.

2.4 Electrochemical section

The electrochemical properties of $MgSrZn_xFe_2O_4$ nanoparticles were studied in a three-electrode system with 1M Na_2SO_4 as the electrolyte and nickel foam (NF) as the current collector. The working electrode was prepared by mixing 80 wt.% active material, 15 wt.% conductive carbon and 5 wt.% PVDF binder. The obtained slurry was coated on the pre-cleaned Ni foam with an active material loading of about 2 mg and then dried at 80 °C for overnight. EC characterizations including CV, GCD and EIS were performed at room temperature to investigate the charge-storage performance, rate ability and interface features of the electrodes.

3 Result and Discussion

3.1 TG/DTA and XRD analysis

Fig. 2(a-c) depicts the TGA/DTA of the $MgSrZn_xFe_2O_4$ precursor powders (x = 0.00, 0.10 and 0.20). The thermal breakdown properties of the $MgSrZn_xFe_2O_4$ precursor powders were studied by TGA/DTA. The TGA curves show a slow reduction of the residual mass with temperature and then a zone of relatively constant mass at high temperature. The weight loss in temperatures below around 187 °C is mainly associated with the removal of physically adsorbed moisture and volatile substances. The mass loss at 621 °C can be attributed to the decomposition of metal hydroxide and other species originated from precursors acquired during the NaOH assisted co-precipitation process. The rather stable residual mass after this temperature range indicates the completion of the main breakdown processes and the formation of thermally stable oxide compounds. The corresponding DTA curves show wide thermal effects in the whole studied temperature range, which can be attributed to dehydration, decomposition of the precursor and subsequent crystallisation of the ferrite phase. The composition $MgSrZn_{0.2}Fe_2O_4$ showed the least mass loss, whereas $MgSrZn_{0.1}Fe_2O_4$ showed the greatest total weight loss among the compositions evaluated. The higher mass loss at x=0.20 may be ascribed to the larger amount of thermally decomposable hydroxylated and

precursor derived entities formed during the NaOH-assisted co-precipitation process. However, the decreased mass loss of the x = 0.10 sample reflects a relatively lesser retention of volatile and hydroxyl-bearing compounds. All specimens exhibit pretty stable residual masses above about 650–700°C indicating the end of the main breakdown reactions. The above results indicate that the excess temperatures over the primary breakdown zone are suitable for the subsequent calcination to obtain a crystalline ferrite phase.

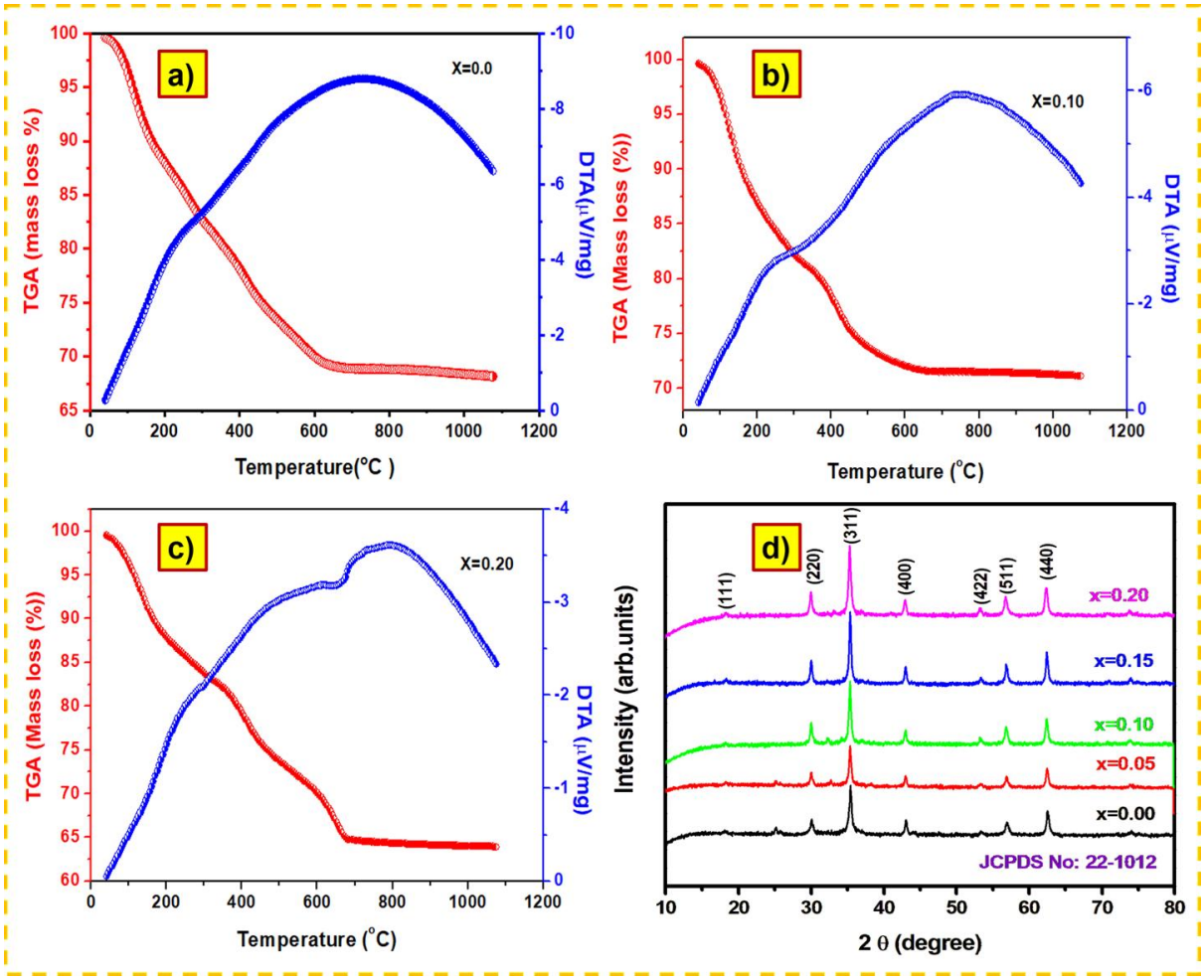

Fig 2 (a-c) TGA/DTA graph of $MgSrZn_{0.2}Fe_2O_4$ (X=0.00, 0.10 and 0.20) material; (d) XRD pattern of $MgSrZn_{0.2}Fe_2O_4$ (X=0.00, 0.05, 0.10, 0.15 and 0.20) materials.

The XRD was used to study the crystalline structure of the prepared $MgSrZn_xFe_2O_4$ samples (Fig. 2d). The characteristic peaks are observed at roughly 18.2°, 30.0°, 35.2°, 42.8°, 53.1°, 56.6°, and 62.2° for all the compositions (x = 0.00, 0.05, 0.10, 0.15, and 0.20) corresponding to the (111), (220), (311), (400), (422), (511), and (440) planes accordingly. These reflections are characteristic of cubic spinel ferrite configuration and are in good agreement with the reference pattern of $ZnFe_2O_4$ (JCPDS No. 22-1012) [32]. No other

significant diffraction peaks were detected, indicating that no crystalline secondary phases were identified within the detection limits of the XRD measurement. The presence of the characteristic spinel reflections for all Zn concentrations indicates that the basic cubic spinel structure is maintained with compositional changes. The little changes in the maximum strength and position are ascribed to the modification of the lattice parameters, crystallite size and the distribution of cations by the substitution of Zn.

3.2 FTIR analysis

Fig. 3 represents the FTIR spectra of $MgSrZn_xFe_2O_4$ ferrites. The characteristic metal–oxygen vibrations are observed in all the spectra in the 583.57 cm^{-1} region [33].

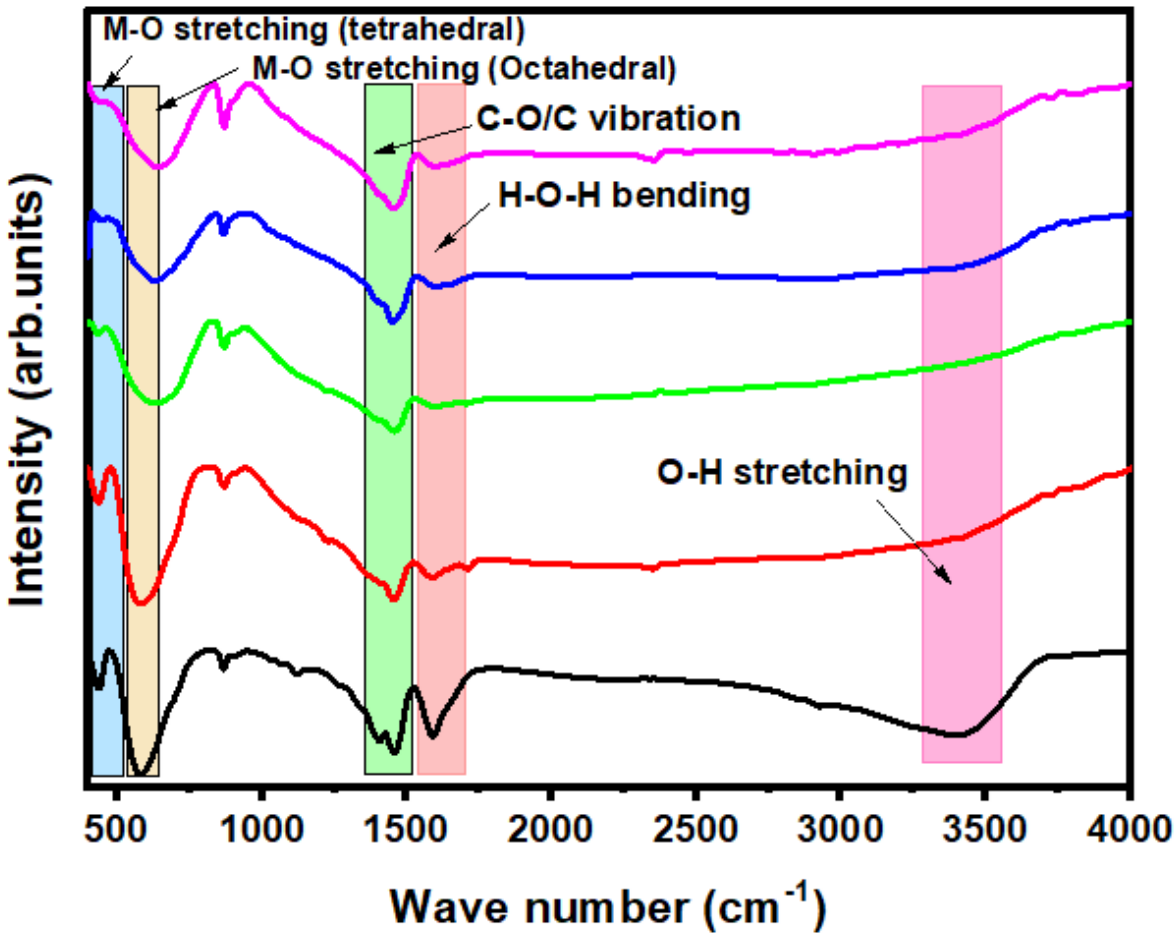

Fig. 3 FTIR spectrum of $MgSrZn_{0.2}Fe_2O_4$ (X=0.00, 0.05, 0.10, 0.15 and 0.20) materials.

The higher wavenumber band (583.57 cm^{-1}) is often attributed to M-O stretching vibrations for cations in tetrahedral positions while the lower wavenumber band (435.36 cm^{-1}) corresponds to vibrations related to octahedral sites characteristic of the spinel ferrite structure [34, 35]. The broad band at about 3419.18 cm^{-1} is attributable to the O-H stretching of the

surface hydroxyl groups and the absorbed moisture [36]. The peak at 1595.48 cm^{-1} is mostly related with the H-O-H bending of the adsorbed water [37]. Weak bands in the 1460 cm^{-1} range can be assigned to surface carbonate species [38]. The small changes in the M-O vibrational bands with increasing Zn content can be due to the changes in the local metal-oxygen environments and the organization of lattice/cations. However, the precise cation distribution of the tetrahedral and octahedral sites cannot be predicted by FTIR alone. The FTIR results together with the XRD study confirm that the characteristic ferrite metal-oxygen structure is maintained throughout the compositional range studied.

3.3 SEM and EDS analysis

The surface morphology of prepared $MgSrZn_xFe_2O_4$ ferrites was studied by FESEM and is shown in Fig. 4(a-e) for x = 0.00, 0.05, 0.10, 0.15 and 0.20 accordingly.

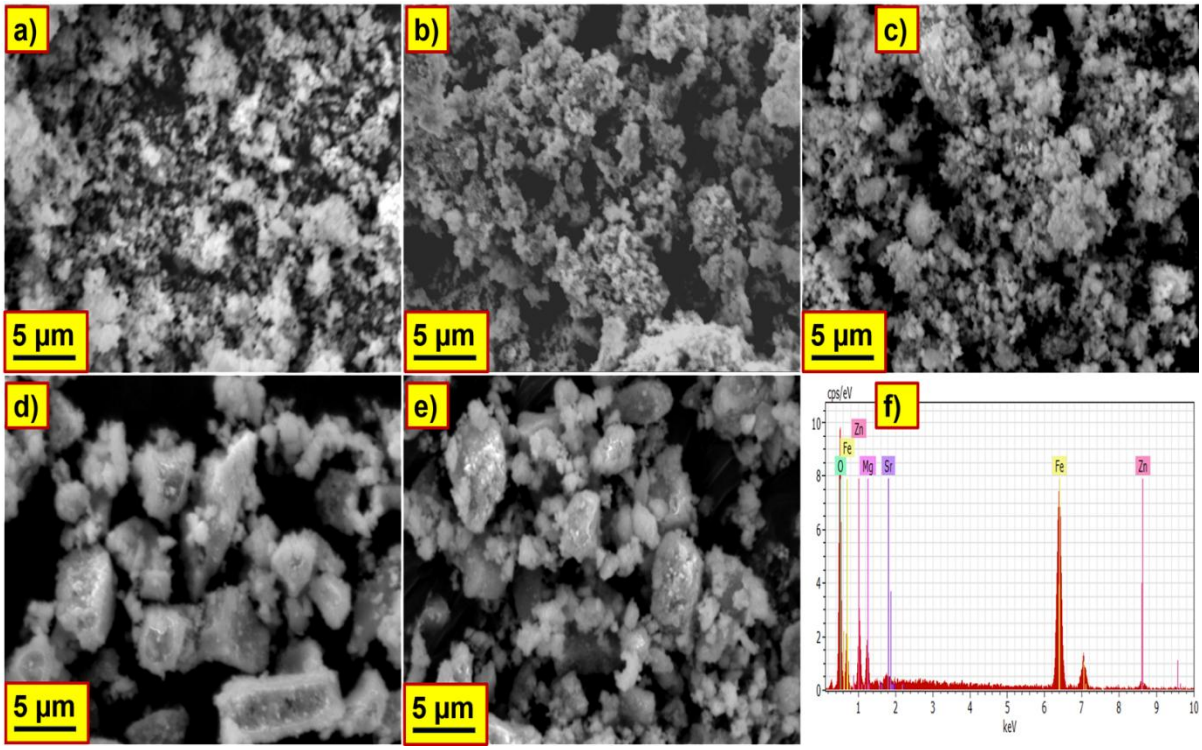

Fig 4 SEM images of $MgSrZn_{0.2}Fe_2O_4$ (a) X=0.00; (b) 0.05; (c) 0.10; (d) 0.15; (e) and 0.20); (d) EDS analysis of $MgSrZn_{0.2}Fe_2O_4$ (x=0.10) material.

In all formulations, the particles morphologies are largely non-uniform and clustered, due to the high surface energy and interparticle forces of the ferrite crystals. A morphologically interesting distinction is observed in the $MgSrZn_{0.15}Fe_2O_4$ sample [Fig. 4(d)] with the presence of long-rod structures coupled with irregularly agglomerated particles. This morphological change can be ascribed to the change of the nucleation and crystal growth kinetics due to the

inclusion of Zn in the Mg-Sr ferrite matrix. For x = 0.20 [Fig. 4(e)] the structure is mostly of an uneven and agglomerated shape. Therefore, the rod-like structure appears to be more well-developed at the intermediate Zn concentration of x = 0.15. The present FESEM photos were taken with a scale bar of 5 μm, hence these features are tentatively called rod-like formations rather than nanorods; to confirm that they are nanoscale, higher magnification FESEM or TEM would be required. EDS analysis confirms the presence of Mg, Sr, Zn, Fe and O, which are the expected constituent elements of the $MgSrZn_{0.15}Fe_2O_4$ system. The characteristic Fe and Zn signals are particularly evident, together with the corresponding Mg, Sr and O signals. No significant foreign-element peaks are observed in the presented spectrum, supporting the formation of the desired multicomponent ferrite phase.

3.4 VSM analysis

The magnetic characteristics of $MgSrZn_xFe_2O_4$ (x = 0.00-0.20) were studied by room temperature vibrating sample magnetometry (VSM).

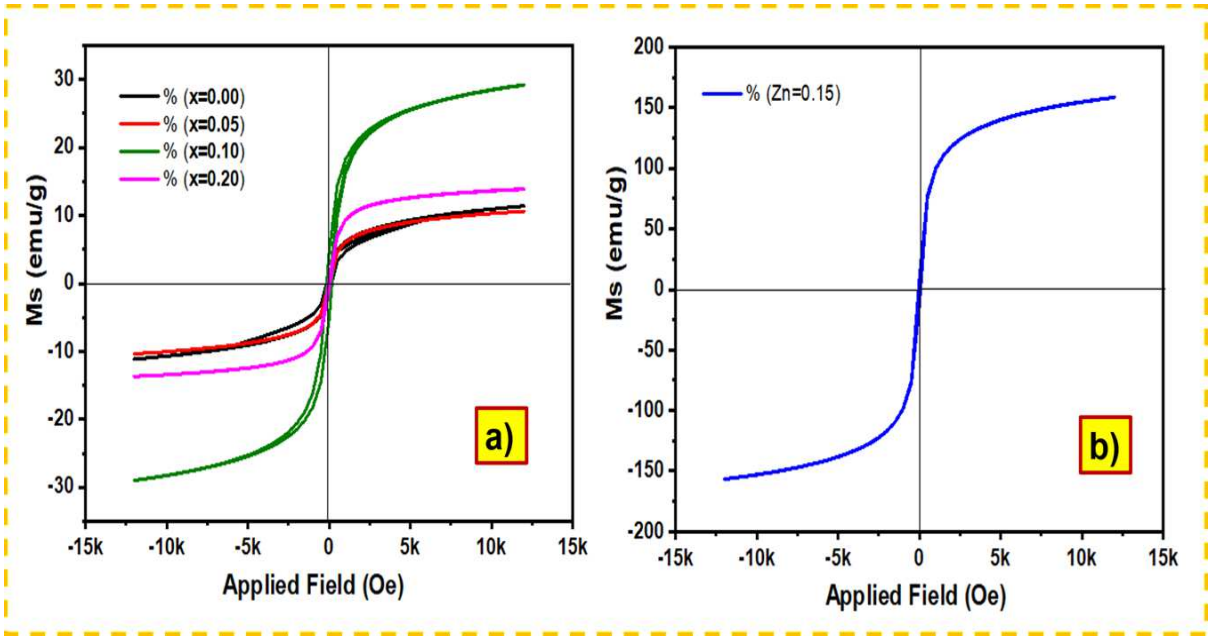

Fig. 5 VSM analysis of $MgSrZn_{0.2}Fe_2O_4$ (a) X=0.00, 0.05, 0.10, and 0.20 ; (b $MgSrZn_{0.2}Fe_2O_4$ (x=0.15).

The accompanying hysteresis loops show the clear magnetic hysteresis, which confirms the ferromagnetic/ ferrimagnetic features of the synthesised ferrite samples. The hysteresis loops provide values for the saturation magnetisation (Ms), remanent magnetisation (Mr) and coercive field (Hc). These data are summarised in Table X. The values of Ms, Mr and Hc for the undoped $MgSrZn_xFe_2O_4$ sample (x = 0.00) were found to be 11.272 $emug^{-1}$, 1.5482 $emug^{-}$

[1] and 164.44 G, respectively. The magnetic characteristics exhibited interesting features on substitution of Zn. M_s showed a slight drop to 10.492 $emug^{-1}$ at x = 0.05, while Hc decreased significantly to 81.563 G. With increasing Zn inclusion, M s increased to 29.108 $emug^{-1}$ for x=0.10. It is noteworthy that the x = 0.15 formulation showed a considerable increase in M s to 157.53 emu g. However, its H c decreased to 67.599 G. At x = 0.20, M s decreased again to 13.786 emu g and H c further decreased to 61.917 G. Therefore, the replacement of Zn leads to a non-linear change in magnetic properties in which the maximum saturation magnetisation was found in the composition x = 0.15 and the minimum coercive field was found in the sample x = 0.20.

Material	**Ms (emu g^{-1})**	**Hc (oe)**	**Key magnetic observation**	**Ref**
$Mg_{0.5}Zn_{0.5}Fe_2O_4$	102	~28	Zn-induced cation redistribution strongly modifies magnetization	39
Nd-doped $Mg_{0.5}Zn_{0.5}Fe_2O_4$	32.19-23.71	221.53-156.77 (Decreased with Nd)	Transition from harder to softer magnetic behavior	40
$CoFe_2O_4$	476-80	-	Annealing atmosphere strongly changes M_s through cation migration/oxygen vacancies	41
$CoFe_2O_4$	75	40	High M_s with relatively low Hc for coated/NP system	42
$MnFe_2O_4$	30.25 at 300K	15.10 at 300K	Soft magnetic behavior	43
$NiFe_2O_4$	37.96	91.69	Spinel Ni ferrite prepared by oxidation roasting	44
$CoFe_2O_4$	51.60 at 300K	146.01 at 300K	Stronger magnetic anisotropy than Mn ferrite	43
$Zn_{0.2}Co_{0.8}Fe_2O_4$	37.16	0.209 (soft magnetic)	Zn addition reduces coercivity of Co ferrite	45
$SrFe_{12}O_{19}$	59.68	-	Hard magnetic M-type ferrite	46

Nb–Zn doped $SrFe_{12}O_{19}$	79.33	Increased by 18.5%	Zn/Nb substitution enhances M_s through Fe-site modification	16
$MgSrZn_{0.15}Fe_2O_4$	157.53	67.60	Highest Ms, Low Hc	**This work**

3.5 Electrochemical analysis

The electrochemical properties of the optimized $MgSrZn_{0.15}Fe_2O_4$ electrode were investigated in an aqueous solution of 1 M Na_2SO_4 using a three-electrode system. Figure 6(a) shows the cyclic voltammograms recorded in the potential range of 0-0.5 V at scan velocities from 5 to 100 mVs^{-1}. The CV profiles show a progressive increase in the current response with increasing scan rate, suggesting a fast electrochemical reaction of the electrode. At the higher scan rate, the CV curves maintain their general shape, demonstrating a good reversibility of the charge-storage mechanism. The increase in the enclosed CV area with scan rate is consistent with the increase in the charge-storage contribution at high scan rates. The kinetics of charge storage was clarified by studying the relationship between peak current (i) and scan rate (v) using the power-law equation [47],

$$i = av^b \quad \text{----------(1)}$$

where a is a constant and v^b is the kinetic parameter. The b-value of the anodic peak is 0.555 with R^2 value of 0.9704 as shown in Fig. 6(b). Correspondingly, the cathodic peak gives a b-value of 0.507, with a R^2 value of 0.9810 as shown in Fig. 6(c). Both values are close to 0.5 indicating that the electrochemical charge-storage mechanism is dominated by the diffusion-restricted ion movement and not by an optimum surface-controlled capacitive process. The small deviation from 0.5 implies that the influence of surface-controlled or pseudocapacitive mechanisms can also be taken into account. The calculated specific capacitance based on the CV curves decreases gradually from 156 F g^{-1} at 5 mV s^{-1} to 45 F g^{-1} at 100 mV s^{-1} (Fig. 6(d)). The decrease in capacitance at high scan rates is attributed to the insufficient time for Na^+ ions to diffuse deeply into the electrochemically active portions of the electrode. Thus, only the conveniently accessible surface and near-surface active sites are important for charge storage at high scan speeds. In contrast, a low scan rate provides sufficient

time for the diffusion of electrolyte ions into the electrode matrix and the activation of more electroactive sites leading to higher specific capacitance.

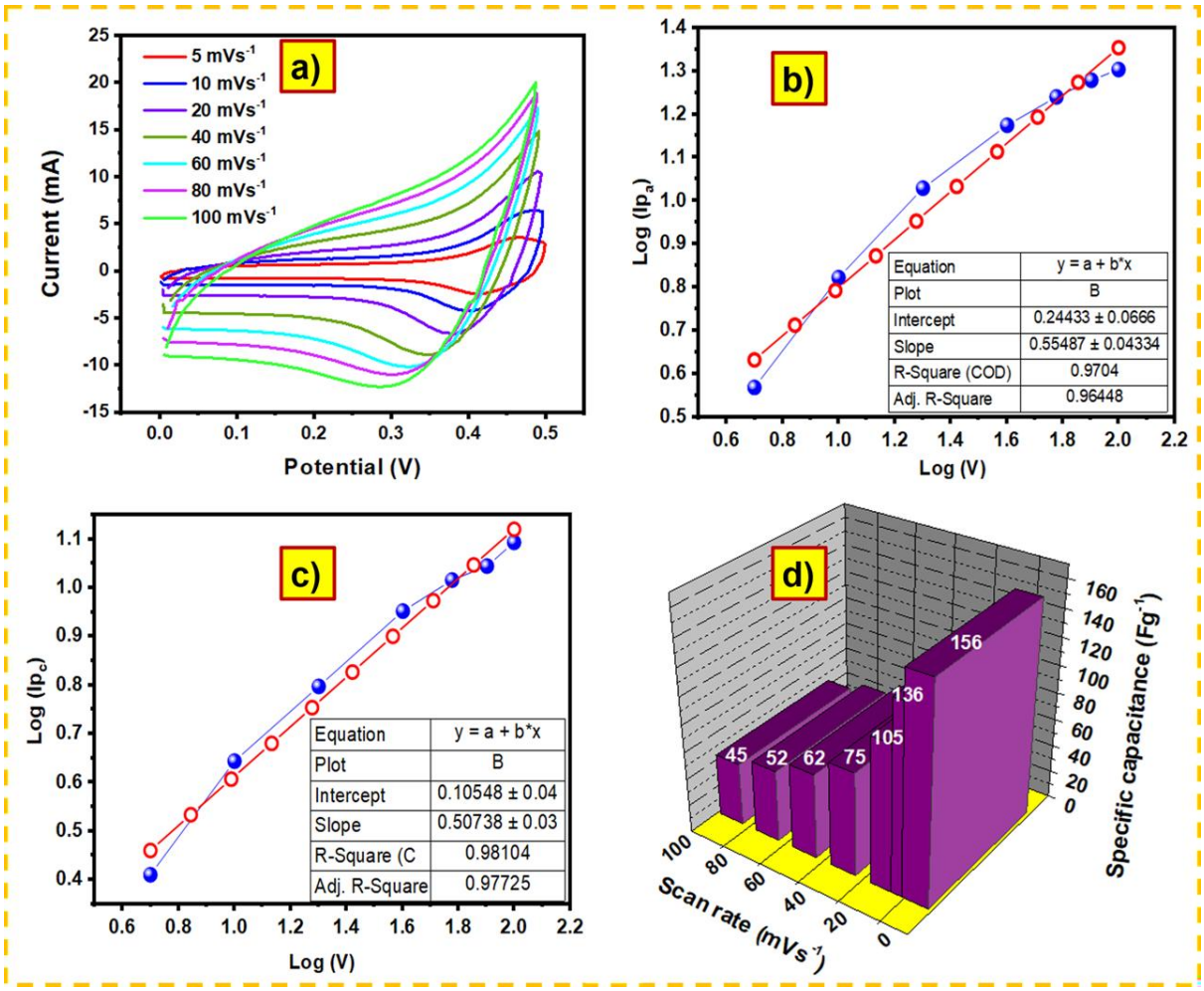

Fig. 6 Electrochemical analysis of $MgSrZn_{0.2}Fe_2O_4$ (X=0.15) electrode; (a) CV analysis of $MgSrZn_{0.2}Fe_2O_4$ (X=0.15) electrode; (b) Anodic b values plotted by Log V versus Log Ip_a of $MgSrZn_{0.2}Fe_2O_4$ (x=0.10) electrode; (c) Cathodic b values plotted by Log V versus Log Ip_c of $MgSrZn_{0.2}Fe_2O_4$ (x=0.10) electrode; (d) $MgSrZn_{0.2}Fe_2O_4$ (x=0.10) electrode specific capacitance values of different scan rate.

The Trasatti analysis using the capacitance data with the scan rate clarified the charge-storage mechanism of $MgSrZn_{0.15}0Fe_2O_4$ electrode. The graph of (1/C) versus ($v^{1/2}$) is shown in Fig. 7(a). The plot shows a strong linear dependence with (R^2 = 0.99123), which can be explained by the Trasatti equation [48],

$$(1/C = 1/C_{\text{total}} + k\, v^{1/2}) \text{ ----------(2)}$$

The resulting y-intercept of 0.0011 F g^{-1} corresponds to ($1/C_{total}$), leading to a projected total capacitance of around 909.1 F g^{-1}. The gradient of 0.002 is the kinetic constant k for the response dependent on the scan rate.

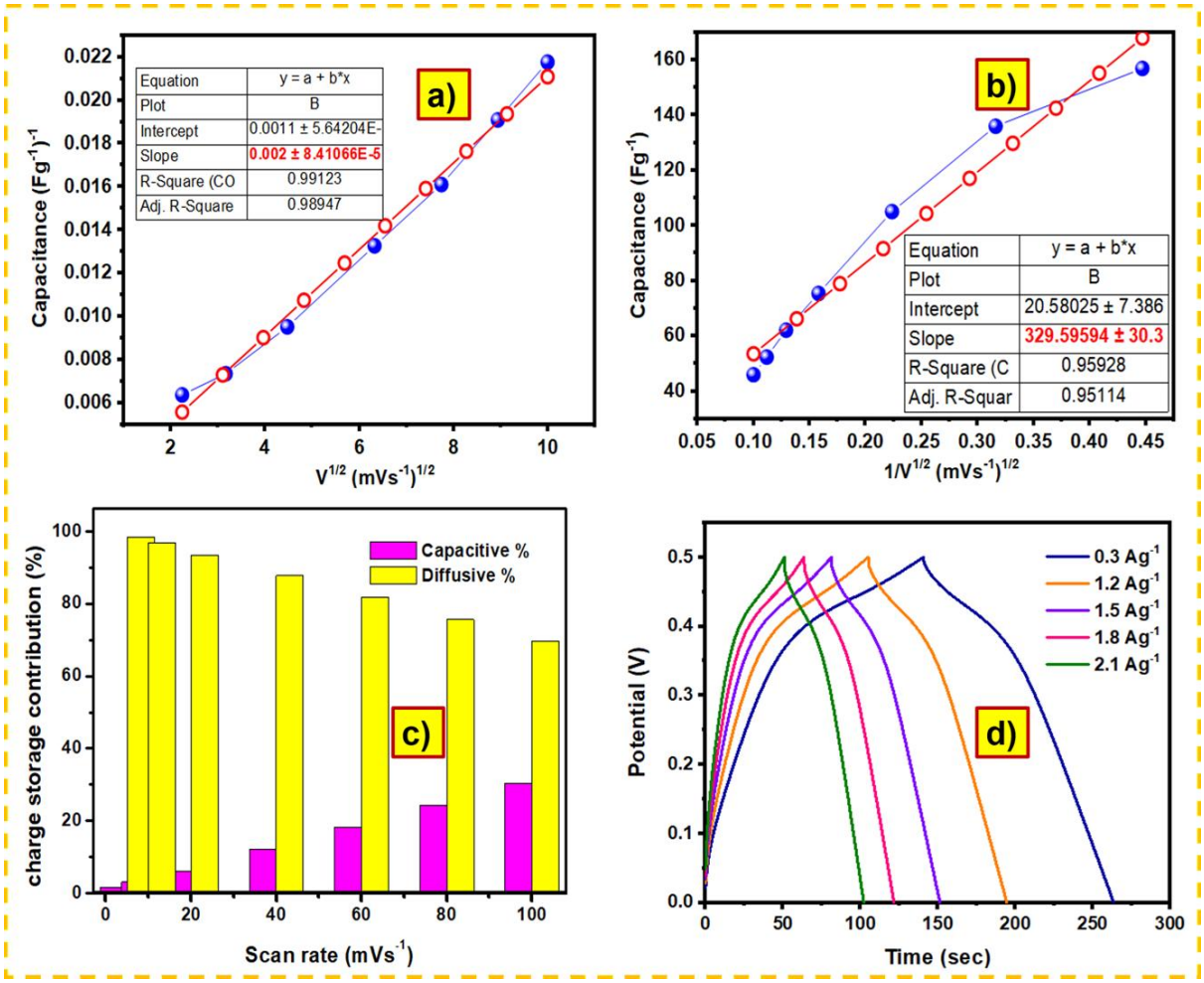

Fig. 7 (a) Capacitive contribution plotted by $V^{1/2}(mVs^{-1})^{1/2}$ versus 1/Capacitance (Fg^{-1}) of $MgSrZn_{0.2}Fe_2O_4$ (x=0.10) electrode; (b) Total capacitance plotted by $1/V^{1/2}(mVs^{-1})^{1/2}$ versus Capacitance (Fg^{-1}) of $MgSrZn_{0.2}Fe_2O_4$ (x=0.10) electrode; (c) Bar diagram of $MgSrZn_{0.2}Fe_2O_4$ (x=0.10) electrode capacitive and diffusive contribution (%); (d) GCD result of $MgSrZn_{0.2}Fe_2O_4$ (x=0.10) electrode.

Furthermore, the complementary graph of C vs. $1/v^{1/2}$ shown in Fig. 7(b) exhibits good linearity (R^2=0.95928) and the y-intercept value of the graph indicate an outer/surface-accessible capacitance of 20.58 F g^{-1}. The inner/diffusion-based capacitance is estimated to be 888.52 F g^{-1} from equation

$$C_{inner} = C_{Total} - C_{outer} \quad \text{----------(3)}$$

Therefore, the external and internal contributions calculated are around 2.26% and 97.74%, respectively, which suggests that the charge-storage properties of $MgSrZn_{0.1}0Fe_2O_4$ are mostly associated with the electrochemically accessible ion movement into the internal active sites. The large internal capacitance component implies that the porous and active electrode architecture provides ample access to electrolyte ions beyond the external surface. The capacitive and diffusion-controlled contributions at different scan rates are further shown in Fig. 7(c), which further demonstrates the increasing contribution of the surface-controlled charge storage in high scan rates, while the diffusion-controlled storage is still dominant. This behavior is attributed to the shorter time for the electrolyte ions to diffuse into the inner electroactive regions at higher scan rates. The diffusion-controlled effect is improved, as the electrolyte ions can access interior active areas at low scan speeds. As seen in Fig. 7(d), the GCD profiles exhibit a slow decrease of discharge durations with increasing current density confirming the expected decrease of available charge-storage capacity at high rates.

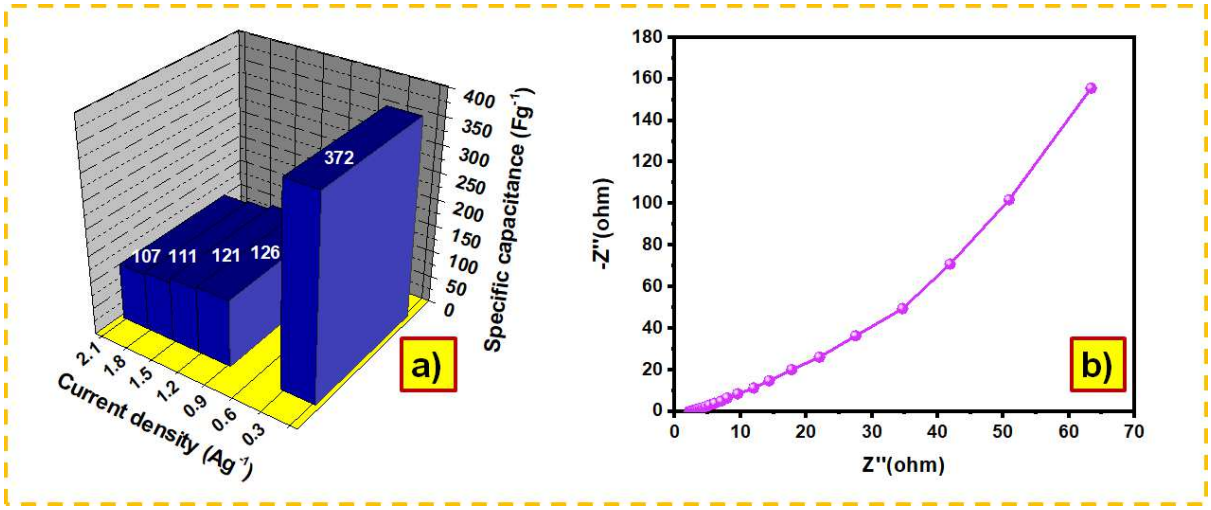

Fig.8 (a) $MgSrZn_{0.2}Fe_2O_4$ (x=0.10) electrode specific capacitance values of different current density; (b) EIS analysis of $MgSrZn_{0.2}Fe_2O_4$ (x=0.10) electrode.

The galvanostatic charge discharge (GCD) behaviour of $MgSrZn_{0.15}0Fe_2O_4$ electrode was investigated at different current densities and the corresponding specific capacitance values are depicted in Fig. 8(a). The electrode exhibits a maximum specific capacitance of 372 F g^{-1} at a 0.3 A g^{-1} The specific capacitance decreases to 126, 121, 107 and 111 F g^{-1} at 0.6, 0.9, 1.2 and 1.5 A g^{-1} with the increase of current density. The electrochemical impedance spectroscopy (EIS) was applied to study the interfacial charge-transfer and ion-transport features of the $MgSrZn_{0.15}0Fe_2O_4$ electrode, and the Nyquist plot is shown in Fig. 8(b). The impedance response exhibits a low frequency region resembling a near vertical line indicative of

predominantly capacitive features and efficient ion transport at the electrode/electrolyte interface. The high frequency intersection with the real axis corresponds to the equivalent series resistance (Rs) which sums up the resistance of the electrolyte, the electrode material and the electrical contacts. Any semicircular feature in the high- to intermediate- frequency region relates to the interfacial charge-transfer resistance (Rct). The capacitive nature in the low frequency region exhibits good electrolyte-ion transport and electrochemical charge storage processes in the $MgSrZn_{0.15}Fe_2O_4$ electrode.

4 Conclusion

To summarize, we have systematically studied the ferrites $MgSrZnxFe_2O_4$ with x = 0.00, 0.05, 0.10, 0.15 and 0.20 in an effort to find out the effect of Zn substitution on their morphological, elemental, magnetic and electrochemical features. FESEM investigation showed mostly irregular and aggregated particles, however the $MgSrZn_{0.15}Fe_2O_4$ sample had also elongated rod-like features, suggesting a composition-dependent morphological evolution. The EDS test revealed the presence of Mg, Sr, Zn, Fe and O in the synthesized ferrite system. The VSM results show a considerable change in the magnetic properties with Zn content. The maximum saturation magnetization of 157.53 emu g^{-1} with a coercivity of 67.60 Oe is found for $MgSrZn_{0.15}Fe_2O_4$. Moreover, the $MgSrZn_{0.15}Fe_2O_4$ electrode exhibited good electrochemical charge storage properties in 1 M Na_2SO_4 electrolyte with specific capacitance of 271 F g^{-1} at a scan rate of 5 mVs^{-1} from cyclic voltammetry and 372 F g^{-1} at a current density of 1.5 A g^{-1} from galvanostatic charge-discharge. The Trasatti analysis identified a major diffusion-controlled factor and the kinetic analysis suggested a growing contribution of surface-controlled mechanisms with increasing scan rate. The results demonstrate that the substitution of Zn is an effective approach to modify the magnetic and electrochemical properties of the $MgSrZnxFe_2O_4$ ferrites. The composition with x = 0.15 showed promising electrochemical charge-storage behavior and improved magnetic performance. These results suggest the possibility of using Zn-doped Mg-Sr ferrites in several magnetic and electrochemical applications.

Funding

The authors declare that no funds, grants, or other support were received during the preparation of this manuscript.

Data availability

The datasets generated and/or analysed during the current study are available from the corresponding author on reasonable request.

Declaration of interests

The authors declare that they have no known competing financial interests or personal relationships that could have appeared to influence the work reported in this paper.

Reference

1. M. Armand, J.M. Tarascon, "Building better batteries," Nature, 451, 652-657, 2008.
2. . Chu, A. Majumdar, "Opportunities and challenges for a sustainable energy future," Nature, 488, 94-303, 2012.
3. Z. Yang, J. Zhang, M.C.W. Kintner-Meyer, X. Lu, D. Choi, J.P. Lemmon, J. Liu, "Electrochemical energy storage for green grid," Chem. Revs, 111, 3577-3613, 2011.
4. Y. Gogotsi, P. Simon, "True performance metrics in electrochemical energy storage," Science, 334, 917-918, 201
5. C. Liu, F. Li, L.P. Ma, H.M. Cheng, "Advanced materials for energy storage," Advanced Materials, 22, E28-E62, 2010.
6. P. Simon, Y. Gogotsi, "Materials for electrochemical capacitors," Nature Materials, 7, 845-854, 2008.
7. J.R. Miller, P. Simon, "Electrochemical capacitors for energy management," Science, 321, 651-652, 2008.
8. A. Burke, "Ultracapacitors: why, how, and where is the technology," Journal of Power Sources, 91, 37-50, 2000.
9. G. Wang, L. Zhang, J. Zhang, "A review of electrode materials for electrochemical supercapacitors," Chem. Soc. Revs, 41, 97–828, 2012.
10. M. Winter, R.J. Brodd, "What are batteries, fuel cells, and supercapacitors?" Chem. Revs, 104, 4245-4270, 2004.
11. M. Vangari, T. Pryor, L. Jiang, "Supercapacitors: review of materials and fabrication methods," J. Energy. Eng, 39, 72-79, 2013.
12. Y. Wang, Y. Song, Y. Xia, "Electrochemical capacitors: mechanism, materials, systems, characterization and applications," Chem. Soc. Revs, 45, 5925-5950, 2016.

13. V.G. Harris, A. Geiler, Y. Chen, S.D. Yoon, M. Wu, A. Yang, Z. Chen, P. He, P.V. Parimi, X. Zuo, C.E. Patton, M. Abe, O. Acher, C. Vittoria, "Recent advances in processing and applications of microwave ferrites," J. Magnet. Magnet. Mater, 321, 2035-2047, 2009.
14. A. Goldman, Modern Ferrite Technology, Springer, New York, 2006.
15. S. Sugimoto, M. Masuda, H. Nakamura, M. Homma, "Magnetic properties of ultrafine ferrite particles," J. Magnet. Magnet. Mater, 196-197, 104-106, 1999.
16. A.M. Bagwan, S.S. Bagwan, U.V. Shembade, A.R. Sonkawade, P.G. Raje, S.D. Ghongade, S.J. Shinde, R.B. Bagwan, M.R. Waikar, A.V. Moholkar, S.A. Masti, R.G. Sonkawade, "Enhancing the performance of supercapacitors with chemically synthesized spinel magnesium ferrite: investigating the influence of current collectors," J. Mater. Sci: Mater. Electro, 36, 1-16, 2025.
17. N.K. Gaikwad, V.S. Kumbhar, "Facile synthesis of spinal ferrite $MgFe_2O_4$ nanoparticles via combustion route as a promising electrode for supercapacitor applications," Mater. Res. Express, 10, p. 075504, 2023.
18. A.M. Bagwan et al., "Enhancing the performance of supercapacitors with chemically synthesized spinel magnesium ferrite: investigating the influence of current collectors," J. Mater. Sci: Mater. Electro, 36, 1–16, 2025.
19. M. Manohar, T. Suvarna, S.V.P. Vattikuti, J.P. Goud, B.A. Al-Asbahi, S.M.H. Qaid, K.H. Kim, "Investigating the potential of $Mg_{0.1}ZnxCu_{0.5-x}Fe_2O_4$ nanoparticles for energy storage applications," Mater. Sci. Semiconductor. Proces, 185, 108897, 2025.
20. M. Sharma, "Combustion synthesis, spectral and electrochemical characterization of chromium-doped magnesium ferrite ($MgFe_2O_4$) nanoparticles for enhanced supercapacitor electrode performance," J. Phy. Chem.Solid, 198, 112476, 2025.
21. S. Patil, S. Deshmukh, "Cation redistribution in governing charge transfer and oxygen evolution activity via Zn^{2+} and Ni^{2+} substitution in $CoFe_2O_4$ spinel ferrites," J. Electroanalytical. Chem, 972, 116800, 2024.
22. R. Kumar, P. Singh, "Enhancing electrochemical supercapacitor performance of $MgFe_2O_4$ spinel nanostructures through palladium doping," Intern. J. Hydro. Energy, 48, 2150-2162, 2023.
23. M. Sharma, "Combustion synthesis, spectral and electrochemical characterization of chromium-doped magnesium ferrite ($MgFe_2O_4$) nanoparticles for enhanced supercapacitor electrode performance," J. Phys. Chem. Solid, 198, 112476, 2025.

24. S. Patil, S. Deshmukh, "Cation redistribution in governing charge transfer and oxygen evolution activity via Zn^{2+} and Ni^{2+} substitution in $CoFe_2O_{44}$ spinel ferrites," Journal of Electroanalytical Chemistry, 972, p. 116800, 2024.
25. A. Ullah, "Synthesis and characterization of $Zn_{0.5}Mg_{0.5}Fe_2O_4$ nanoparticles for energy storage applications," M.S. thesis, National University of Sciences and Technology, Islamabad, Pakistan, 2023.
26. X. Zhang, L. Wang, Q. Li, "Zn^{2+}-doped $BaFe_{12}O_{19}$ nanoplates exhibit superior cycling performances for advanced lithium-ion batteries," RSC. Advs, 5, 78945-78952, 2015.
27. M. Manohar, T. Suvarna, S.V.P. Vattikuti, J.P. Goud, B.A. Al-Asbahi, S.M.H. Qaid, K.H. Kim, "Investigating the potential of $Mg_{0.5}ZnxCu_{0.5-x}Fe_2O_4$ nanoparticles for energy storage applications," Mater. Sci. Semicondu. Process, 185, 108897, 2025.
28. D.S. Nikam, S.M. Rathod, S.R. Gawali, "The structural, electrical and magnetic properties of Co^{2+} content dependent Mg-Sr nanoferrite for electromagnetic induction," Ceram. Inter, 43, 16845-16853, 2017.
29. M. Manohar, T. Suvarna, S.V.P. Vattikuti, J.P. Goud, B.A. Al-Asbahi, S.M.H. Qaid, K.H. Kim, "Investigating the potential of $Mg_{0.5}Zn_xCu0.5\text{-}xFe_2O_4$ nanoparticles for energy storage applications," Mate. Sci. Semiconduc. Process, 185, p. 108897, 2025.
30. S. Patil, S. Deshmukh, "Cation redistribution in governing charge transfer and oxygen evolution activity via Zn^{2+} and Ni^{2+} substitution in $CoFe_2O_4$spinel ferrites," J. Electroanalytical. Chemy, 972, p. 116800, 2024.
31. D.S. Nikam, S.M. Rathod, S.R. Gawali, "The structural, electrical and magnetic properties of Co^{2+} content dependent Mg-Sr nanoferrite for electromagnetic induction," Ceram. Intern, 43, 16845-16853, 2017.
32. C.Y. Tsay, T.T. Ho, Hydrothermally Synthesized Spinel Nanoferrites as Magnetically Separable and Recyclable Visible-Light Photocatalysts for Degradation of Hydrophilic Organic Pollutant. Catalysts, 16(6), (2026) 531.
33. L.F. Vargas, H. Salazar-Tamayo, C.A. Barrero, Structural, morphological and magnetic properties of MFe_2O_4 (M= Mg, Zn and Ni) synthesized by solid state reaction. Interacs, 246(1), (2025) 64.
34. H.N. Chaudhari, P.N. Dhruv, S.S. Meena, S. Kavita, C.B. Basak, N. Patni, C. Chauhan, R.B. Jotania, Effect of annealing temperature on structural, microstructural, and Mössbauer properties of $MgFe_2O_4$ ferrite for photo anode application. J. Sol-Gel. Sci. Techn, 117(3), (2026) 77.

35. B.M. Bindushree, G. Chavan, L.R. Naik, R.F. Bhajantri, V. Gudihal, Effect of yttrium doping on the physical properties of Mg-Zn ferrite: A detailed study. Next Mater, 9, (2025) 101247.
36. A.M. Bagwan, S.S. Bagwan, U.V. Shembade, A.R. Sonkawade, P.G. Raje, S.D. Ghongade, S.J. Shinde, R.B. Bagwan, M.R. Waikar, A.V. Moholkar, Enhancing the performance of supercapacitors with chemically synthesized spinel magnesium ferrite: Investigating the influence of current collectors. J. Mater. Sci. Mater. Electron. 2025, 36, 1654.
37. A.V. Gongal, D.V. Nandanwar, D.S. Badwaik, S.S. Wanjari, V.S. Harode, S.M. Suryawanshi, Study on multifunctional magnesium copper zinc spinel ferrite nanoparticles prepared by hydrothermal route; physical, electrical, and anti-microbial investigation. Nano-Struc. Nano-Objec, 39, (2024) 101248.
38. S. Ali, O.M. Hemeda, F. Elhussiny, M.H. Mahgoub, S. Mohammed, A. Elmekawy, Structural, optical, and magnetic characterization of Cu–Zn–Ni spinel ferrite nanoparticles with antibacterial potential. Sci. Report, 16(1), (2026) 3053.
39. A.M., Nayak, S., Sahu, M., Jagličić, Z., Koželj, P. and Kim, H.J., Cationic redistribution induced magnetic properties of Zn^{2+} substituted $MgFe_2O_4$ spinel ferrite. Phy. B: Conden. Matter, 668, (2023) 415245.
40. R.Y. Mudi, V.B.G. Tiruveedhi, S, Y. Mulushoa P.S.V. Shanmukhi, J.S. Chohan, K.M. Batoo, M.F. Ijaz, Impact of Nd^{3+} doping on $Mg_{0.5}Zn_{0.5}Fe_2O_4$ nano-ferrite: structural, morphological, electrical resistivity, and magnetic properties. South African J. Chem. Eng, 53(1), (2025) 476-482.
41. B.S. Ragunath, A. Thileeba, K.P. Meher, K. Chinnathambi, A. Sathya, Structural and Magnetic Properties of Vacuum and Air annealed $CoFe_2O_4$ Nanoparticles. Sol. Sta. commu, (2025) 116107.
42. S. Ozer, N. Dogan, S. Canim-Ates, A. Bingolbali, Synthesis and characterization of coated $CoFe_2O_4$ nanoparticles with biocompatible compounds and in vitro toxicity assessment on glioma cell Lines. Adv. Mater. Interf, 12(5), (2050) 2400613.
43. T.T.N. Nha, S.H. Prakash, S. Mohana Roopan, J.J. Samuel, D.N. Toan, D.T. Khan, D.D. Bich, T.D. Thanh, L.T.T. D.H. Manh, P.T. Phong, Microwave-assisted co-precipitation synthesis of MFe_2O_4 nanoferrites (M= Co and Mn) using biogenic coir extract and their physical characterization. RSC adv. 15(36), (2025) 29571-29592.
44. J. Wen, J. Yang, C. Liu, Z. He, L. Gao, Synthesis and magnetic properties of spinel $NiFe_2O_4$ nanoparticles by oxidation roasting technique. Mater. Sci. Eng: B, 319, (2025) 118375.

45. B. Sahu, K.V. Ramesh, S.L. Pandrangi, D. Venkatesh, B.P. Singh, P. Chittineedi, S.S. Meena, Study and evaluation of $Zn_{0.2}Co_{0.8}Fe_2O_4$ nanocrystalline spinel ferrites for antimicrobial and anticancer applications. ACS omega, 10(30), (2025) 33192.
46. R.D. Mao, X. Zhang, Y.L. Li, M. Lan, W.N. Ren, S.J. Huang, X. Chang, B.J. Wang, Y. Jiao, L.Z. Li, X.H. Wu, Tailoring magnetic properties of $SrFe_{12}O_{19}$ ferrites through Dy–Ni Co-substitution: a comprehensive study. Ceram. Inter, 50(2), (2024) 3139-3150.
47. S. Xie, P. Fu, L. Wang, H. Gong, F. Wang, F. Chen, Z. Sun, J. Fan, Y. Zhang, J. Zhang, B. Shen, Nb-Zn Co-doping cooperative modulating Fe^{3+} magnetic moment arrangement to enhance the saturation magnetization of strontium ferrite. (2025) Ceram. Intern.
48. M. Silambarasan, R. Boopathiraja, N. Prabhu, S. Manimegalai, T. Keerthana, G. Ramalingam, S. Nirmaladevi, Hydrothermal synthesis of $Ni_2P_2O_7$ nanosheets like efficient electrode for supercapacitor applications: capacitive and diffusive mechanism of Trassati method. J. Inorg. Organo. Polym. Mater, 35(9), (2025) 7364-7379.